hydrology

MDPI

Research Article

Supplementary Materials

Hydrodynamic Parameter Estimation for Simulating Soil-Vegetation-Atmosphere Hydrology Across Forest Stands in the Strengbach Catchment

Benjamin Belfort *, Aya Alzein, Solenn Cotel, Anthony Julien and Sylvain Weill

S1. Meteorological analysis

To better understand the meteorological variability of the periods selected for the implementation of the method, we plotted in Figures S1 (for precipitation) and S2 (for temperature) the monthly precipitation totals and mean monthly temperatures for the four calibration periods, relative to the average values over the entire period from October 2007 to September 2025.

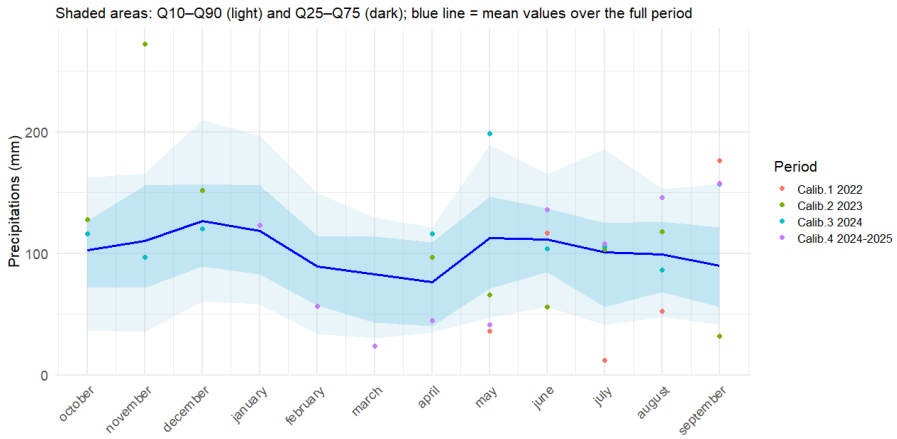


Figure S1. Evolution of average monthly precipitation (blue line) and its variability (shaded areas) over the period from October 2007 to September 2025. The specific monthly values for the selected calibration periods are shown as colored dots.

 https://doi.org/10.3390/hydrology13010011

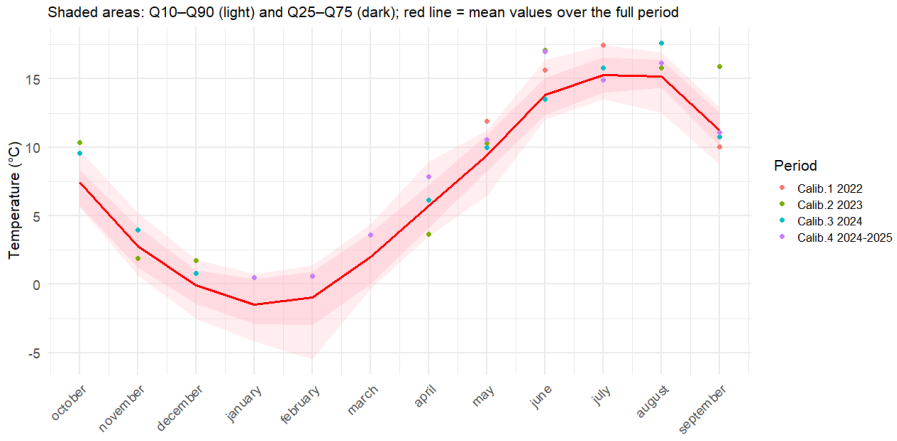


Figure S2. Evolution of average monthly temperature (red line) and its variability (shaded areas) over the period from October 2007 to September 2025. The specific monthly values for the selected calibration periods are shown as colored dots.

S2. Description of the BILHYDAY model

Using a conceptual framework, the BILHYDAY model simulates the water dynamics within the soil–tree–atmosphere system on a daily timestep. Potential evapotranspiration is computed using the Penman method accordingly to Brochet-Gerbier approach. Incoming precipitation first interacts with the canopy, which retains part of it up to a maximum interception capacity; transpiration is then modeled in relation to potential evapotranspiration, available soil water, and leaf area index. The vertical distribution of transpiration across soil depths follows the root density profile. Soil evaporation depends on incident energy derived from direct radiation and an extinction coefficient. The soil column is represented by vertically arranged reservoirs, where drainage proceeds stepwise from upper to lower layers according to their respective field capacities. The top layer receives the portion of precipitation that passes through the canopy and also experiences evaporative losses. Water uptake by roots, linked to transpiration demand, is allocated across soil layers in proportion to root density. Readers interested in this modeling approach may refer to the developments carried out by INRAE Nancy, which provides an online tool available at: https://appgeodb.nancy.inrae.fr/biljou/fr/

Table S1. Parameters implemented in the BILHYDAY model for the spruce (JP) and beech (HET) plots obtained from prior studies and site-specific measurements.

Plots	LAI (-)	budburst and senescence (DOY)	Nb of layers (-)	Roots (%)
JP	3.6	0-365	5	90 (first 30 cm)
HET	4.2	125-300	3	90 (first 70 cm)

As stated in the manuscript, BILHYDAY is employed as a pre-processing tool to compute AET values and to derive the upper boundary flux conditions shown in Figures 3b and 4b. For completeness, we provide in this Supplementary Information the cumulative AET values for the different seasons; this allows us to highlight differences between the two study plots that arise from physiological contrasts between beech and spruce under this mid-elevation forest setting.

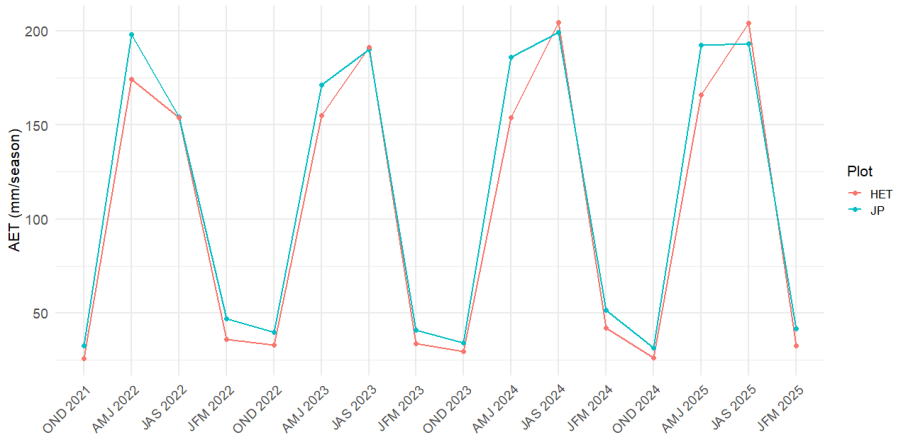


Figure S3. Seasonal evolution of cumulative AET for the spruce (JP, shown in red) and beech (HET, shown in green) plots at the Strengbach catchment.

S3. Summary of the numerical methodology and results of parameter estimation

S3.1. Short overview of the numerical methodology

A graphical summary of the methodology is provided in Figure S4. This representation helps clarify how the different models are combined. The preliminary step (Step 1) concerns data preparation, including both WC sensor data and the meteorological and granulometric datasets. Note that this step also provides an initial parameter set derived from the PTF (ROSETTA) approach. Some of these parameters are subsequently corrected to account for stoniness. In Step 2, BILHYDAY is used for AET preprocessing, which serves to define the upper boundary condition. In Step 3, the WAMOS-IPE-1D code is employed for parameter estimation using an inverse modeling approach at an hourly time step, over 4 calibration periods for the spruce plot (3 periods for the beech plot). For each parameter set, the algorithm optimizes the three parameters (K_s, α, n) by minimizing the differences between simulated and observed hourly values (see Eq. (13)). The WAMOS-1D code is then applied in Step 4 for direct modeling using the different parameter sets obtained in Step 3. This final step aims to evaluate the simulation performance and select the overall best parameter set for each plot.

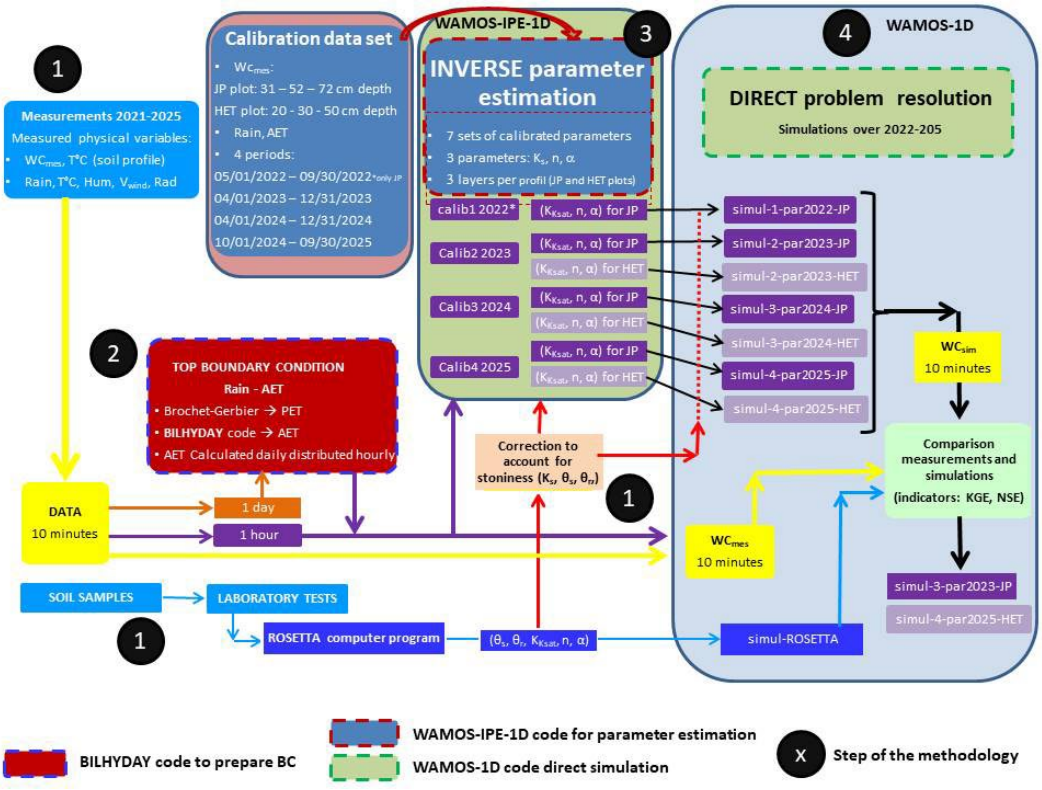


Figure S4. Graphical representation of the numerical methodology.

S3.2. Results of parameter estimation

Tables S2 and S3 describe the results of parameter estimation for the spruce and beech plots, respectively. The different techniques investigated are reported, including the inversion of four parameters and the use of Rosetta PTFs. Figures S5 and S6 illustrate the corresponding parameter sets and show how they relate to each other according to the estimation technique.

Table S2. Parameters obtained for the spruce plot throughout the various techniques. Index i (1 to 3) refers to the soil layer: 1 = 0-35cm, 2 = 35-65cm, 3 = 65-110cm.

Layer 1	$K_{s,1}$ ($cm.d^{-1}$)	α_1 (cm^{-1})	n_1 (-)	$\Theta_{s,1}$ ($cm^3.cm^{-3}$)	$\Theta r_{,1}$ ($cm^3.cm^{-3}$)
JP2-1	61.09	0.0068	1.6694	0.4074	0.0461
JP2-2	29.25	0.0065	1.6687	0.4074	0.0461
JP2-3	110.76	0.0064	1.6530	0.4074	0.0461
JP2-4	176.48	0.0063	1.6558	0.4074	0.0461
JP2-Rosetta	36.42	0.0060	1.6132	0.4074	0.0461
Inv_4P_JP2-3	152.76	0.0064	1.6389	0.3961	0.0461

Layer 2	$K_{s,2}$ ($cm.d^{-1}$)	α_2 (cm^{-1})	n_2 (-)	$\Theta_{s,2}$ ($cm^3.cm^{-3}$)	$\Theta r_{,2}$ ($cm^3.cm^{-3}$)
JP2-1	54.04	0.0092	1.5392	0.3580	0.0384
JP2-2	23.35	0.0091	1.4959	0.3580	0.0384
JP2-3	28.96	0.0089	1.5329	0.3580	0.0384
JP2-4	31.24	0.0085	1.5209	0.3580	0.0384
JP2-Rosetta	26.76	0.0095	1.5521	0.3978	0.0427
Inv_4P_JP2-3	27.99	0.0094	1.5434	0.3942	0.0427

Layer 3	$K_{s,3}$ ($cm.d^{-1}$)	α_3 (cm^{-1})	n_3 (-)	$\Theta_{s,3}$ ($cm^3.cm^{-3}$)	$\Theta r_{,3}$ ($cm^3.cm^{-3}$)
JP2-1	12.70	0.0045	1.6485	0.3360	0.0036
JP2-2	47.30	0.0034	1.6001	0.3360	0.0036
JP2-3	28.85	0.0043	1.6483	0.3360	0.0036
JP2-4	15.87	0.0042	1.6468	0.3360	0.0036
JP2-Rosetta	29.60	0.0045	1.6817	0.4200	0.0045
Inv_4P_JP2-3	101.24	0.0046	1.6677	0.4155	0.0045

https://doi.org/10.3390/hydrology13010011

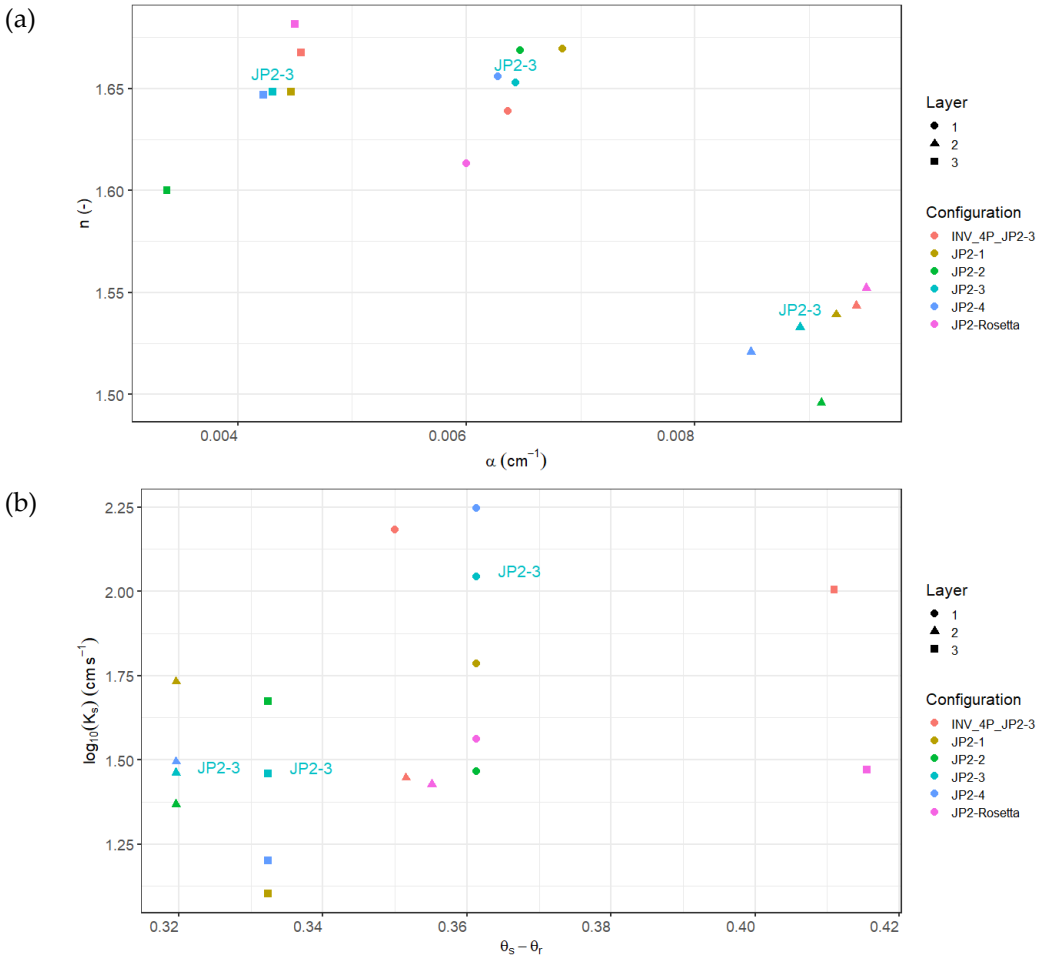


Figure S5. Hydrodynamic parameters obtained using different estimation techniques for the JP plot. Symbols represent the three soil layers, and colors distinguish the techniques. **(a)** representation of n vs α; **(b)** representation of log(Ks) vs (θs – θr).

Table S3. Parameters obtained for the beech plot throughout the various techniques. Index i (1 to 3) refers to the soil layer: 1 = 0-25cm, 2 = 25-45cm, 3 = 45-100cm.

Layer 1	$K_{s,1}$ ($cm.d^{-1}$)	α_1 (cm^{-1})	n_1 (-)	$\Theta_{s,1}$ ($cm^3.cm^{-3}$)	$\Theta r_{,1}$ ($cm^3.cm^{-3}$)
HET1-2	1175.06	0.0129	4.4956	0.3872	0.0581
HET1-3	18.30	0.0048	1.6890	0.3872	0.0581
HET1-4	19.68	0.0049	1.6982	0.3872	0.0581
HET1-Rosetta	18.36	0.0046	1.6676	0.4302	0.0645
Inv_4P_HET1-4	89.13	0.0046	1.7203	0.3695	0.0581

Layer 2	$K_{s,2}$ ($cm.d^{-1}$)	α_2 (cm^{-1})	n_2 (-)	$\Theta_{s,2}$ ($cm^3.cm^{-3}$)	$\Theta r_{,2}$ ($cm^3.cm^{-3}$)
HET1-2	124.83	0.0166	3.6032	0.3498	0.0487
HET1-3	31.99	0.0045	1.6998	0.3498	0.0487
HET1-4	40.91	0.0045	1.7085	0.3498	0.0487
HET1-Rosetta	23.38	0.0044	1.6927	0.4373	0.0609
Inv_4P_HET1-4	1513.38	0.0045	1.7246	0.3405	0.0487

Layer 3	$K_{s,3}$ ($cm.d^{-1}$)	α_3 (cm^{-1})	n_3 (-)	$\Theta_{s,3}$ ($cm^3.cm^{-3}$)	$\Theta r_{,3}$ ($cm^3.cm^{-3}$)
HET1-2	50.50	0.0462	1.8656	0.2675	0.0322
HET1-3	32.72	0.0040	1.6660	0.2675	0.0322
HET1-4	27.47	0.0039	1.6472	0.2675	0.0322
HET1-Rosetta	35.37	0.0044	1.7139	0.4459	0.0537
Inv_4P_HET1-4	31.07	0.0047	1.6104	0.2710	0.0322

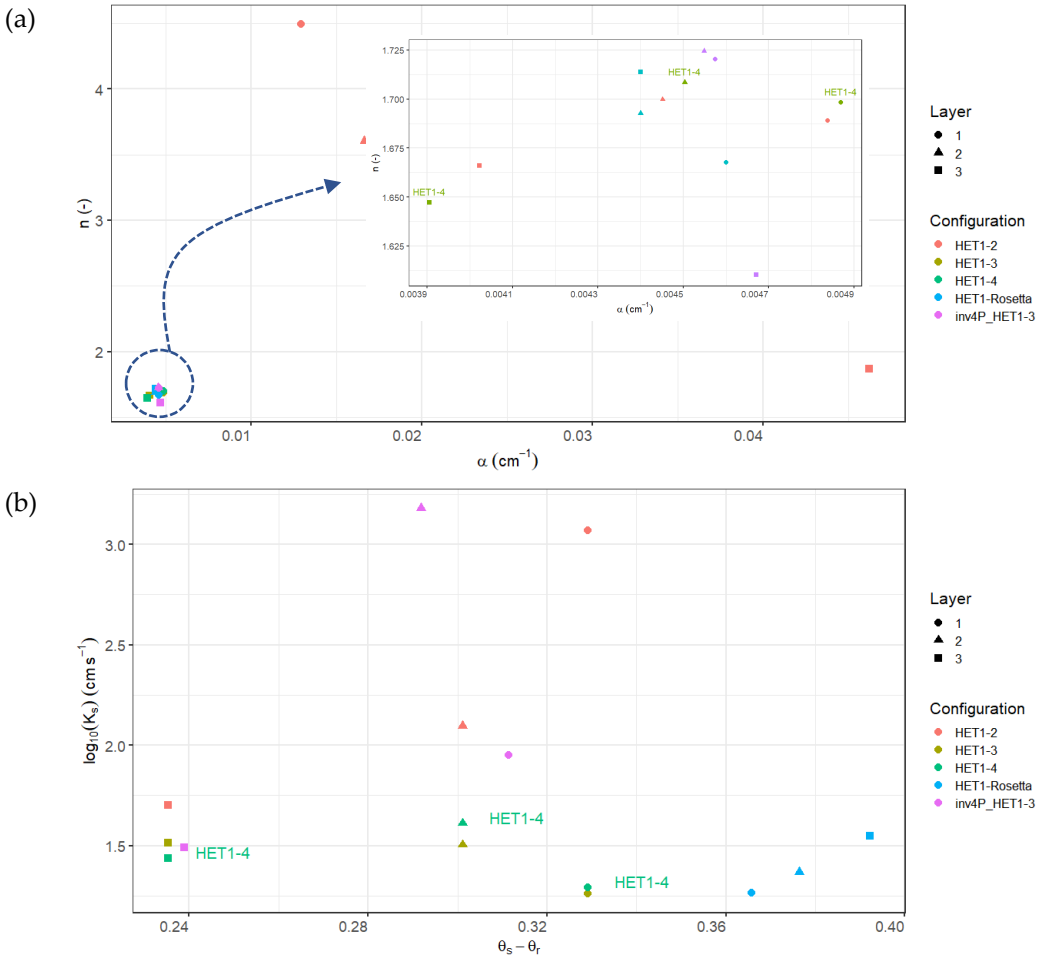


Figure S6. Hydrodynamic parameters obtained using different estimation techniques for the HET plot. Symbols represent the three soil layers, and colors distinguish the techniques. **(a)** representation of n vs α with a zoomed-in window; **(b)** representation of log(Ks) vs (θs – θr).

S4. Efficiency criterion for the various parameter sets

Tables S4 and S5 describe the efficiency criterion obtained for the complete period of simulation where WC data are available, either for each individual layer or for the complete soil profile. Notice that two criteria have been added: the biais (pBiais, Eq. S1) and the root mean square error (RMSE, Eq. S2):

$$pBiais_i = \frac{\sum_{n=1}^{N_{time}} \left(\theta^n_{sim,i} - \theta^n_{meas,i}\right)}{\sum_{n=1}^{N_{time}} \theta^n_{meas,i}} \quad \text{(S1)}$$

$$RMSE_i = \sqrt{\frac{1}{N_{time}} \sum_{n=1}^{N_{time}} \left(\theta^n_{sim,i} - \theta^n_{meas,i}\right)^2} \quad \text{(S1)}$$

Table S4. Efficiency criterion for the different configurations investigated on the spruce plot (JP).

All layers	NSE_{ALL}	KGE_{ALL}	$pBiais_{ALL}$	$RMSE_{ALL}$
JP2-1	0.559	0.707	5.225	0.020
JP2-2	0.566	0.807	-5.301	0.020
JP2-3	**0.671**	**0.831**	**-1.631**	**0.018**
JP2-4	0.595	0.762	5.438	0.020
JP2-Rosetta	0.153	0.742	11.736	0.028
Inv_4P_JP2-3	0.622	0.821	-3.724	0.019

Layer 1	NSE_1	KGE_1	$pBiais_1$	$RMSE_1$
JP2-1	0.679	0.661	2.369	0.021
JP2-2	0.589	0.785	-4.409	0.024
JP2-3	**0.685**	**0.755**	**0.776**	**0.021**
JP2-4	0.641	0.692	4.578	0.022
JP2-Rosetta	0.301	0.681	12.067	0.031
Inv_4P_JP2-3	0.639	0.799	-3.413	0.022

Layer 2	NSE_2	KGE_2	$pBiais_2$	$RMSE_2$
JP2-1	0.578	0.720	2.780	0.014
JP2-2	0.327	0.728	-6.040	0.018
JP2-3	**0.553**	**0.750**	**-3.005**	**0.015**
JP2-4	0.495	0.718	4.598	0.015
JP2-Rosetta	0.390	0.738	5.802	0.017
Inv_4P_JP2-3	0.514	0.768	-2.867	0.015

Layer 3	NSE_3	KGE_3	$pBiais_3$	$RMSE_3$
JP2-1	-0.498	0.701	11.188	0.024
JP2-2	0.165	0.663	-5.597	0.018
JP2-3	**0.306**	**0.688**	**-3.074**	**0.017**
JP2-4	-0.010	0.706	7.343	0.020
JP2-Rosetta	-1.830	0.648	17.528	0.034
Inv_4P_JP2-3	0.165	0.661	-4.988	0.018

https://doi.org/10.3390/hydrology13010011

To visually represent the efficiency of the different configurations, radar charts were provided (see Figures S7 and S8). For this purpose, the various performance indicators were normalized using a standard formula, as detailed in Equation S3, and the pBias and RMSE indicators were reoriented so that their optimum values tend toward 1. $$\text{fct_norm} = \frac{x_i - \min_j(x_j)}{\max_j(x_j) - \min_j(x_j)} \quad \text{(S3)}$$

We also add a global criterion which consists in an arithmetic mean of the other criterion.

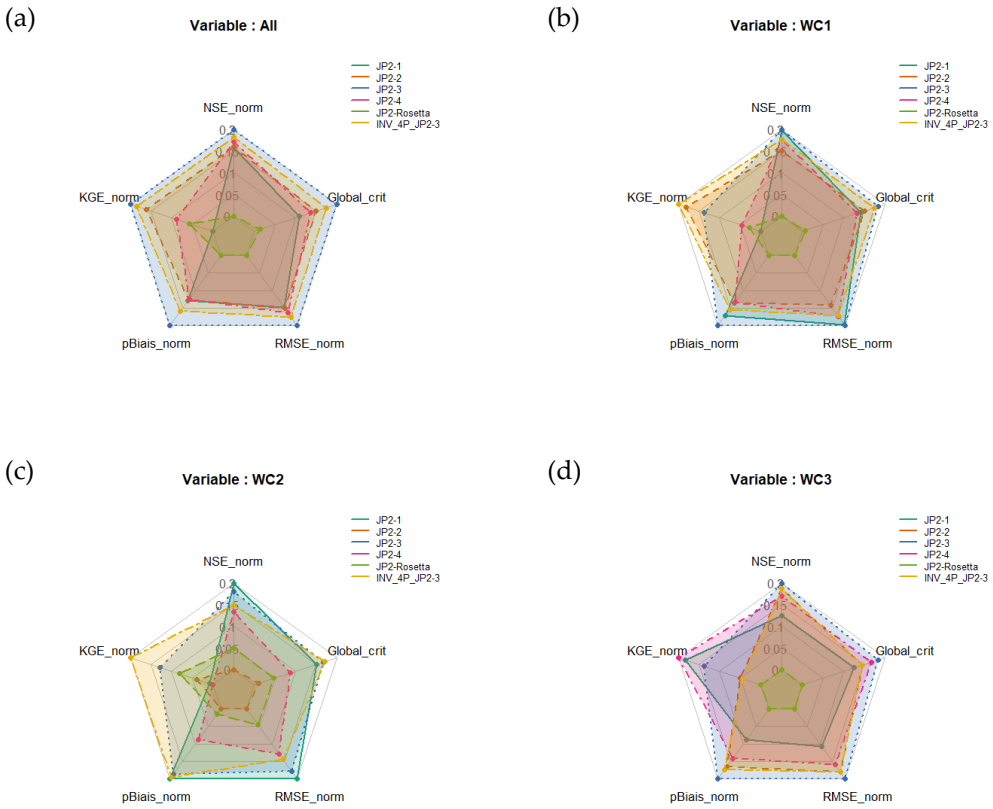


Figure S7. Radar charts illustrating the efficiency of the various estimation techniques applied to the JP plot. **(a)** shows the results for the complete profile; **(b)** for the first layer; **(c)** for the second layer; and **(d)** for the third layer.

Table S5. Efficiency criterion for the different configurations investigated on the beech plot (HET).

All layers	NSE_{ALL}	KGE_{ALL}	$pBiais_{ALL}$	$RMSE_{ALL}$
HET1-2	0.214	0.754	-13.865	0.030
HET1-3	0.647	0.727	2.219	0.020
HET1-4	**0.654**	**0.685**	**2.849**	**0.020**
HET1-Rosetta	-2.748	0.257	38.306	0.066
Inv_4P_HET1-4	0.649	0.638	3.758	0.020

Layer 1	NSE_1	KGE_1	$pBiais_1$	$RMSE_1$
HET1-2	-0.232	0.693	-16.011	0.036
HET1-3	0.522	0.596	2.907	0.023
HET1-4	**0.538**	**0.596**	**2.270**	**0.022**
HET1-Rosetta	-1.082	0.452	23.248	0.047
Inv_4P_HET1-4	0.542	0.513	2.171	0.022

Layer 2	NSE_2	KGE_2	$pBiais_2$	$RMSE_2$
HET1-2	0.365	0.752	-8.235	0.024
HET1-3	0.496	0.495	3.973	0.022
HET1-4	**0.514**	**0.503**	**3.348**	**0.021**
HET1-Rosetta	-3.355	0.321	37.248	0.064
Inv_4P_HET1-4	0.512	0.511	4.136	0.021

Layer 3	NSE_3	KGE_3	$pBiais_3$	$RMSE_3$
HET1-2	-0.651	0.494	-17.716	0.029
HET1-3	0.498	0.517	-0.779	0.016
HET1-4	**0.477**	**0.511**	**3.022**	**0.016**
HET1-Rosetta	-12.369	0.204	59.536	0.083
Inv_4P_HET1-4	0.441	0.521	5.414	0.017

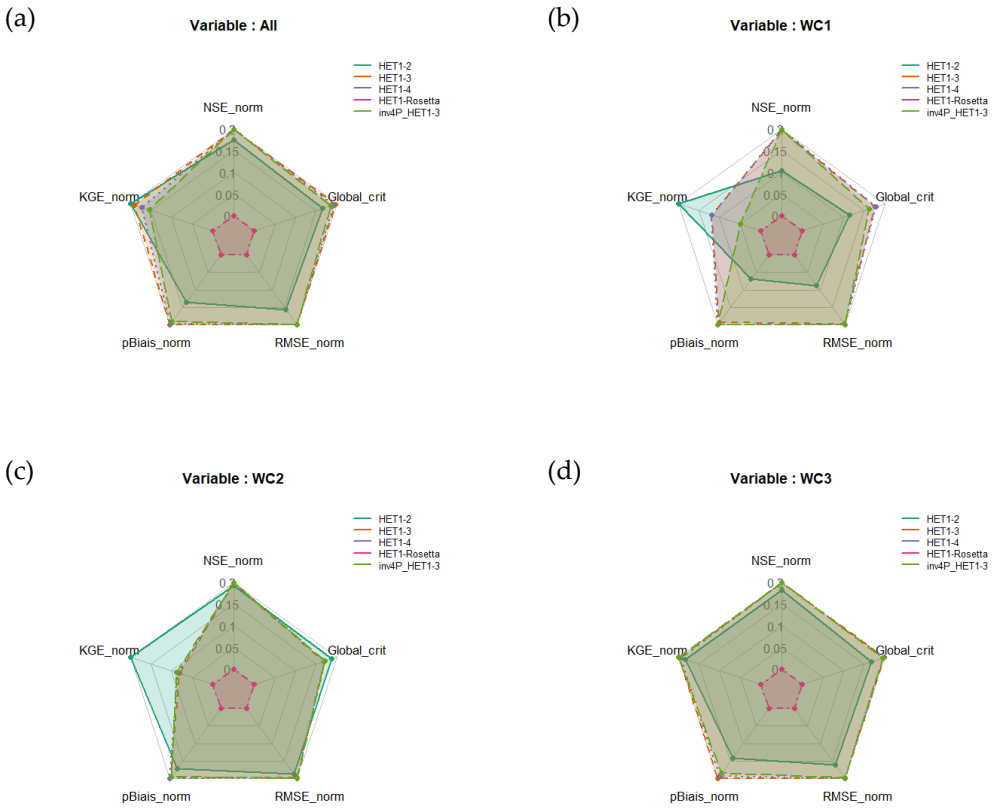


Figure S8. Radar charts illustrating the efficiency of the various estimation techniques applied to the HET plot. **(a)** shows the results for the complete profile; **(b)** for the first layer; **(c)** for the second layer; and **(d)** for the third layer.

https://doi.org/10.3390/hydrology13010011

S5. Soil WC time series

In the main manuscript, in Figure 5b, it may seem somewhat frustrating that the model does not accurately reproduce the drying of the soil during the summer drought episode. A calibration focused on this specific period, as performed with Calibration 2, leads to a better fit, as shown in Figure S9. However, it is also clear that this parameter set is no longer suitable for reproducing other periods of the record. Indeed, this parameter set appears markedly different in the representations shown in Figures S6a and S6b.

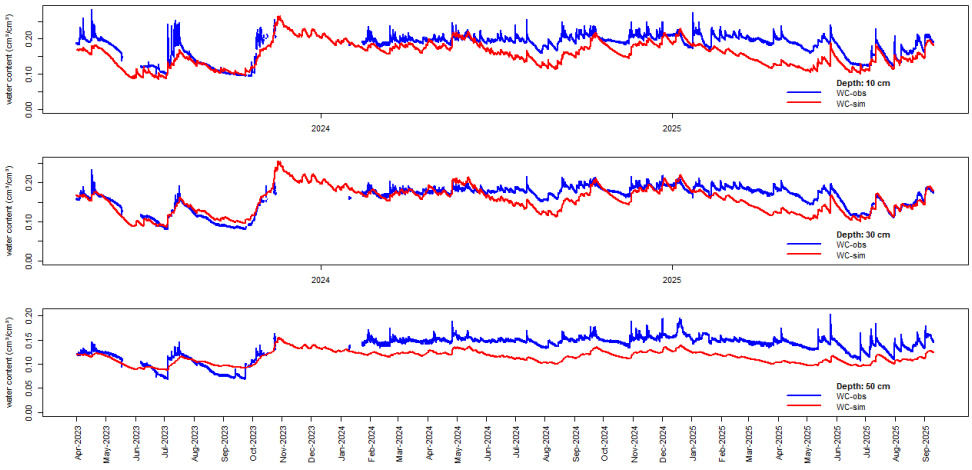


Figure S9. Comparison of soil water content (WC) time series obtained from the model (run with the HET1-2 configuration; red line) and from measurements (blue line) for three soil layers at 31, 52, and 72 cm depth.

https://doi.org/10.3390/hydrology13010011